Letters

Comments on "Theory and Application of Calibration Techniques for an NDBC Directional Wave Measurements Buoy": Nonlinear Effects

D. E. BARRICK, SENIOR MEMBER, IEEE, B. J. LIPA, AND KENNETH E. STEELE

Abstract—**Steele *et al.* [3] present an extensive set of linear calibration techniques that are applied to NDBC wave-buoy sensor spectral output before calculating and disseminating directional wave spectra. We here identify and estimate the nonlinear effects that produce biases still present in the output. These effects are due both to wave nonlinearities themselves and to constraints on the buoy and mooring system to the driving forces. Simple models used here show that these nonlinearities can produce spectral energy biases of 5–15 percent at and above the spectral peak frequency, and even greater errors below it. NDBC presently records wave data from vertically stabilized and fixed accelerometers and slope sensors. Our calculations show that these sensors all incur bias due to wave nonlinearities; this bias is greatest for vertically stabilized accelerometers and is least for slope sensors. Effects of the resulting inconsistencies between the different sensors are most pronounced below the spectral peak where the nonlinear terms dominate; these effects are illustrated with measured data.**

I. Introduction

The pitch/roll wave buoy is more widely accepted and employed than any other instrument for measuring ocean surface wave-height directional information; it has been demonstrated and used since 1955[1]. Ideally, it should follow the surface of the sea, giving a perfect measure of its elevation and slopes from which wave information could then be derived. Such buoys, most frequently configured with discus hulls, have been deployed in a free-drifting mode [2] (requiring a boat standing by for eventual recovery) or with a slack-line mooring [3] to allow unattended operation.

Many factors, related both to the buoy system and the ocean surface itself, conspire to limit the accuracy and utility of this device from obtaining the true wave-height directional spectrum. Considerable attention has been paid to sources of error within the instrument and mooring. Recently, a thorough description of extensive calibration techniques developed and used at the National Data Buoy Center (NDBC) has been published by Steele *et al.* [3]. While the methods presented therein deal with amplitude and phase bias factors at each wave spectral frequency that can be measured and removed, there are other sources of bias that are not so easily removed. The latter originate mainly from nonlinearities introduced from surface currents, the mooring, and the waves themselves. These sources of errors were cited at a U.S. National Research Council Symposium and Workshop in 1981, and efforts to quantify and account for them were recommended [4].

Manuscript received June 15, 1987; revised January 16, 1989. Data used in this work was provided by the National Data Buoy Center under Contract no. DB32189 to Computer Sciences Corporation, with Subcontract no. CSC/ATD-83-C-511 to CODAR Research.

D. E. Barrick and B. J. Lipa are with Ocean Surface Research, Inc., 165 Harcross Road, Woodside, CA 94062.

K. E. Steele is with the National Data Buoy Center, National Oceanographic and Atmospheric Administration, Stennis Space Center, MS 39529.

IEEE Log Number 8928099.

The present note considers the effects of both wave and current/mooring nonlinearities on pitch/roll buoy performance. Through simplified examples we estimate the nature and order of magnitude of errors in the region near the wave-energy spectral peak. These nonnegligible biases are not presently removed from the NDBC or any other measured data. We feel that it is important to point this out, for the directional wave buoy has come to be considered a standard against which other instruments under development should be compared for accuracy. This has occurred naturally because of the device's longevity, its widespread usage, and because NDBC and the U.S. National Weather Service have deployed many of these buoys and disseminates the data obtained from them to the public.

II. Examples and Models of Nonlinearities

The waves and currents acting on a complex-shaped finite-sized buoy constrained by a mooring cause it to respond nonlinearly to the driving forces. An accurate analysis of this problem is very complex, depending specifically on an exact formulation of the hydrodynamic buoy/mooring response as well as a knowledge of the forcing current profile and wavefield. The latter two items vary considerably from day to day and hence are unknown; in fact, the wavefield itself is sought from the instrument. To obtain "order of magnitude" estimates of these biases we use simple models based on reasonable physical processes and assumptions about buoy response.

A. Buoy Response to Wave Nonlinearities

A wave buoy responds differently to nonlinear wavefields than a fixed sensor like a wave staff. We assume in this section that a pitch/roll buoy: i) Floats freely; ii) measures the slope perfectly; and iii) measures the surface elevation perfectly via its vertical acceleration. The latter two responses, of course, assume low-pass filtering or averaging across the (discus) diameter. Similarly, we assume for a strapped-down accelerometer that the surface elevation is measured via the acceleration normal to the wave surface; this acceleration includes both the orbital motion of the buoy as well as the variation of the gravitational component with tilt due to gravity. The slack mooring offers slight constraint (i.e., the buoy does not drift away) to assumption "i" above, but we assume that as a wave passes under the buoy it follows the wave in the orbital manner of any free-floating particle.

The first two terms of the classic periodic Stokes wave [5] represent the simplest wave nonlinearity: the height, slope, and velocity potential at a (horizontally) fixed point X are

$$\eta(x, t) = a \cos \psi + (a\delta/2) \cos 2\psi + aO(\delta^2) \tag{1}$$

$$\eta_x(x, t) = -\delta \sin \psi - \delta^2 \sin 2\psi + O(\delta^3) \tag{2}$$

and

$$\phi(x, z, t) = (a\omega/k)e^{kz} \sin \psi + (a\omega/k)O(\delta^2) \tag{3}$$

where $\psi = kx - \omega t$ is the phase of the wave progressing in the $+x$ direction, with the temporal radian wavenumber ω and spatial wavenumber k related to each other through the phase velocity $c = \omega/k$ and the (deep water) dispersion relation $\omega^2 = gk$, where g is the acceleration of gravity (9.806 m/s^2). $\delta = ak$ is the waveslope

0364-9059/89/0700-0268$01.00

amplitude, and $O(u^n)$ denotes that all remaining terms are of an order at least u^n in the smallness parameter u. The z direction is taken as being upwards from the mean surface.

As this wave passes under the perfect pitch/roll buoy the first two equations above *do not* describe the height and slope it measures *above the first order*. Before developing the outputs of buoy-mounted instruments, we first find the horizontal and vertical displacements of a free-floating particle $X(x, t)$ and $Z(x, t)$ "orbiting" about x. The particle's horizontal and vertical velocities are derived in terms of these velocities at fixed x by expanding the latter in a Taylor series about $x + X$ and $z + Z$ and retaining the lowest three terms. The x and z velocities at the fixed point x are obtained by differentiating the velocity potential (3) with respect to x and z. These particle velocities (with terms retained through the second order in δ) are then integrated with respect to time (the constants of integration are dropped) to give

$$X(x, t) = -a \sin \psi + \delta^2 ct + aO(\delta^2) \tag{4}$$

and

$$Z(x, t) = a \cos \psi + aO(\delta^2). \tag{5}$$

The second term in (4) is the familiar drift of a particle on the surface due to the nonlinear Stokes current, which shows up as a slight nonclosure of the particle orbits (to second order); this term is of course suppressed by the buoy mooring, for the buoy does not drift away. The slope of the water under the buoy likewise is obtained by expanding $\eta_x(x, t)$ in (2) about $x + X$ in order to obtain:

$$Z_x(x, t) = -\delta \sin \psi - (\delta^2/2) \sin 2\psi + O(\delta^3). \tag{6}$$

Now we can give the heights as determined from the instruments mounted on a discus buoy that perfectly execute the orbital position and slope responses of (4)–(6). The double-integrated (with respect to t) output $Zv(x, t)$ of a vertically stabilized accelerometer is a height given by (5) above and repeated here:

$$Zv(x, t) = a \cos \psi + aO(\delta^2). \tag{7}$$

To obtain an elevation from the slope sensor correctly one would integrate the slope of (6) with respect to x, giving

$$Zs(x, t) = a \cos \psi + (a\delta/4) \cos 2\psi + aO(\delta^2).$$

However, this is *not* how the slope-sensor data from the buoy is used in obtaining cross spectra, for a buoy does not measure the spatial wavenumber directly; the *first-order* dispersion equation is used to relate temporal-to-spatial wavenumber, and does the integration by dividing by the resulting spatial wavenumber. For the solitary wave train considered here, the energy at the second harmonic 2ω is thus related to a pseudowavenumber $k_s = (2\omega)^2/g$, and the height that would be obtained from buoy measurements is actually

$$Zs(x, t) = a \cos \psi + (a\delta/8) \cos 2\psi + aO(\delta^2) \tag{8}$$

rather than that obtained from the previous equation; they differ by a factor of two in the second-harmonic term.

Finally, the "displacement" measured by a strapped-down hull-mounted accelerometer is obtained by: i) Double integrating the acceleration normal to the wave surface using (4)–(6); and ii) adding and double integrating the fluctuating acceleration component of gravity $g\{1 - \cos [\tan^{-1} Z_x(x, t)]\}$, sensed by the tilting accelerometer (again omitting constants of integration), to get

$$Zn(x, t) = a \cos \psi + (3a\delta/16) \cos 2\psi + aO(\delta^2). \tag{9}$$

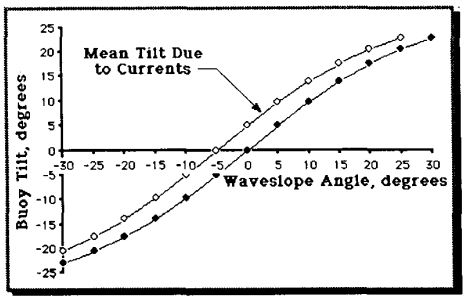

Fig. 1. Slightly nonlinear model used for the buoy tilt-angle response to wave-slope angle, illustrating buoy resistance to capsizing at large wave slopes. Curve with open points includes a mean buoy list of $-5°$ that may result from strong current/wind straining on the mooring.

We note that none of the above three heights measured by perfect buoy-mounted instruments: i) Agree with the true height at a fixed position given by (1) beyond the first order (they underestimate the height); nor do they ii) agree with each other beyond the first order.

B. Nonlinear Buoy-Tilt Restraints

If the discus buoy followed the wave surface perfectly it would encounter breaking waves on occasion that would have vertical slopes. Thin unmoored discus designs [2] respond to these conditions (as they should) by regularly flipping upside down. Large permanently moored buoys of the NDBC design must of necessity avoid the "upside down" condition for obvious functional reasons. Hence the combination of their center of mass, buoyancy, and mooring constrains them so that they follow waveslopes linearly up to a point, beyond which their tilt is limited so that they cannot capsize. Furthermore, currents and winds near the surface which are likely to be strongest during storm conditions when higher slopes are encountered will strain the mooring in a manner to further limit the tilt response to waveslopes. These currents and winds will cause greater tilt constraint along the wind/current direction than across it and will give the buoy a list θ_0 along this direction.

Since this limiting tilt condition is not a sharp cutoff, we model it by the hyperbolic tangent function as

$$\theta = \theta_m \tanh [(\alpha - \theta_0)/\theta_m] \tag{10}$$

where θ is the tilt-angle output from the buoy, θ_m is the maximum tilt that the mooring, currents, and buoy hydrodynamics will allow, θ_0 is the list of the buoy, and α is the true angle of the normal to the wave under the buoy from vertical, related to the slope by $\alpha = \tan^{-1} Z_x(x, t)$. Fig. 1 shows this function plotted for $\theta_m = 30°$, $\theta_0 = 0°$ and $-5°$, where one should keep in mind that typical rms slope angles for even steep waves are less than $10°$. As Fig. 1 shows, the buoy-measured tilt and waveslope angle are equal at small slopes.

Since rms slopes and angles for typical ocean waves are small, we intend to expand all quantities through the third order in δ ,which is the slope amplitude of the sinusoidal waves assumed in (6); e.g., we let $\alpha \cong Z_x - Z_x^3/3$, $\tanh u \cong u - u^3/3$, etc. Finally, we substitute $Z_x(x, t)$ from (6) and expand the powers of trigonometric functions into their harmonics, retaining the lowest-order terms in radian angles and harmonics through the second to obtain

$$\theta \cong \delta_0 - \delta_1 \sin \psi - \delta_2 \sin (2\psi - \xi_2) \tag{11}$$

where $\delta_0 \cong -\theta_0[1 - (\theta_0/\theta_m)^2/3 - \theta_0(\delta/\theta_m)^2/2]$, $\delta_1 \cong \delta[1 - (\theta_0/\theta_m)^2 - (\theta_m^2 - \theta_0^2 + 1)(\delta/2\theta_m)^2]$, $\delta_2 \cong (\delta^2/2)[1 + \theta_0^2(1/2 - \theta_m^2)/\theta_m^4]$, and $\xi_2 \cong \theta_0/\theta_m^2$. Note that if there were no upper limit to the buoy tilt, so that $\theta = \alpha$ (or $\theta_m \to \infty$), and there were no list, so that

$\theta_0 = 0$, then (11) reduces to $\theta \cong Z_x(x, t) = -\delta \sin \psi - (\delta^2/2) \sin 2\psi$, as it should.

III. Discussion of Nonlinear Biases

Because the random ocean surface to the lowest order is a sum of sinusoids (giving rise to a continuous spectrum) rather than the single sinusoid we considered here, the details of the nonlinearities will necessarily be different from our Stokes-wave model. Expressions for second-order nonlinear waves resulting from continuous spectra have been calculated, for example, in [6]–[8]. The *order of magnitude* of the biases they produce, however, are the same and furthermore, the simple models used here allow one to examine qualitively when and where to expect distortions in the sensor spectra. Since realistic waveheight spectra typically have sharp peaks, the ultimate narrow-band representation we have used here—i.e., a single sinusoid—is not that far from reality [8].

In order to meaningfully employ the above model, we choose parameters that are not exaggerated extremes. For tilt restraints we take $\theta_m = 30°$, $\theta_0 = 5°$ as it seems reasonable that the buoy hull and mooring design should not allow tilts beyond 30°. The only nonlinear wave parameter we need is the slope amplitude $\delta = ak$ (the rms slope corresponding to this amplitude is $\delta/\sqrt{2}$). Longuet-Higgins [9] shows that the *maximum* value this parameter can attain is 0.4432. Mechanically generated waves in wave tanks report slope amplitudes as high as 0.3 [9], [10]; when δ is kept less than 0.11, breaking is precluded at the primary frequency [10]. Let us take here $\delta = 0.2$; this gives an rms slope that is nearly the same as the JONSWAP spectrum [11] under developing conditions when waves are breaking. (The spectrum was integrated out to four times the spectral peak frequency to obtain the rms slope.) It corresponds to an rms wave tilt angle of $\sqrt{\langle \alpha^2 \rangle} = 8°$, a condition that certainly should not be considered too extreme. These parameters will then give $\delta_1 \cong 0.92\delta$, $\delta_2 \cong 1.02\ (\delta^2/2)$, and $\xi_2 \Rightarrow 18.2°$.

Comparison of (1) and (7) shows that *the vertically stabilized accelerometer completely omits the second-order nonlinearities* present in the true wave profile. (A similar comparison of (1) and (8), (9) shows that the second-order nonlinear term in the surface elevation obtained from the slope sensors and fixed accelerometer is underestimated by factors of 2 and 8/3, respectively.) Longuet-Higgins arrived at similar conclusions [9] when he studied the accelerations at the surface of a single periodic wave containing *all* nonlinear terms (with the trochoid as its limit). As the sharp crest of this wave passes a fixed point its acceleration tends toward infinity because of the abrupt change in slope across the crest; he showed that a free-floating buoy/particle observes no such sharp spike in acceleration, meaning that the device suppresses the nonlinear contributions. Integrating acceleration twice to obtain the waveheight has the effect of dividing the nonlinear harmonic amplitudes by the square of harmonic frequency, further decreasing their relative contribution to height. *Hence, although a trochoidal wave may have passed beneath the buoy, all it sees is a sinusoid.*

Since the directional spectrum at and near the peak is most important to users, we discuss the region within a factor of two of the peak frequency; this also covers most of the 5–20-s region measurable by NDBC buoys.

A. Beyond the Spectral Peak

The second temporal harmonic of the Stokes wave (for $\delta = 0.2$) is a factor 10 lower in amplitude than the fundamental, as seen in (1); in (spectral) power it is therefore lower by 100. Since (7) shows that the second harmonic is missing entirely from the vertically stabilized accelerometer response to the Stokes wave, the buoy underestimates the true waveheight energy in this region. A continuous spectrum with a Phillips temporal law ω^{-5} will drop by a factor ~ 32 (i.e., 0.03) from the peak to a (frequency) factor of two beyond the peak. Since our Stokes-wave analysis suggests that the nonlinear error at twice the peak is 0.01 of the fundamental spectral energy, the error with respect to the Phillips law may be of the order $0.01/0.03 \cong 30$ percent in this region. Our reasoning here is further supported by the analysis in [12] where a continuous Phillips spectrum is used to calculate the second-order temporal spectral contribution and is shown in [12, fig. 2]. At a factor of 3 beyond the spectral peak the second-order waveheight level is 10 percent of the first order; if the buoy does not respond to second-order wave nonlinearities it will thus be in error by 10 percent. Therefore errors due to nonlinearities in the region which lie at a factor of 2–3 beyond the peak frequency may be expected to produce waveheight energy biases 10–30 percent too low.

B. At the Spectral Peak

The buoy-tilt constraint modeled by (10) and (11), along with our assumed parameters, show that at the fundamental the slope amplitude is 0.92 and hence the slope energy is 0.84 of its true value. The actual directional height energy distribution (in terms of Fourier angular coefficients) depends on accurate, unbiased measurement of both height and slope energy. Hence this can be expected to be in error by 5–20 percent even at and near the spectral peak if the model for tilt constraint considered here is realistic. Direction itself, obtained essentially from the ratio of x-to-y tilt sensor output, will be biased somewhat if the current/wind/wave forcing on the mooring causes different values for θ_0 and θ_m in the two orthogonal directions.

C. Below the Spectral Peak

Although the solitary Stokes wave model produces no energy below the spectral peak, it does show that wavebuoys underestimate the second-order energy present in the wave. Continuous input spectra, however, do produce significant second-order energy below the peak; [12, fig. 2] demonstrates this even though the input first-order spectrum cuts to zero below the peak. Even wave-tank measurements with very narrow-band spectral energy (generated mechanically by a sinusoidally moving piston [10, fig. 2]) show energy at 1/2 the spectral peak frequency, down by a factor of 40 from peak energy.

IV. Support from Measured Data

We examine data measured by a NDBC buoy (Discus Hull 10D4) at Site 46025 (46/25) off Port Hueneme, California, during the Spring of 1986. The calibration methods described in [3] have been applied. In particular, the signal time series from the various instruments were weighted with the parabolic window [3]. Because windows (or the absence thereof) in spectral estimation can deposit energy from a dominant peak (via sidelobes) at other frequencies where the true energy is low, one must be sure such effects do not bias the interpretation of data. Two assurances are offered: i) At the regions away from the spectral peaks examined here the sidelobe levels produced by the parabolic window are predicted to be many dB below the signal levels analyzed; ii) the same window was applied to data from all instruments over the same time periods and hence any sidelobe effect remaining in the data from different instruments at the same frequencies will cancel when their ratios are taken, as they are here. Also, we note that a fixed slope-to-height hull calibration factor measured for each frequency was applied (as described in reference [3]) over all data sets, i.e., this factor was not recalculated and changed versus time for each observation period; this is the only meaningful way to examine nonlinear effects that will vary versus time based on the wave intensity.

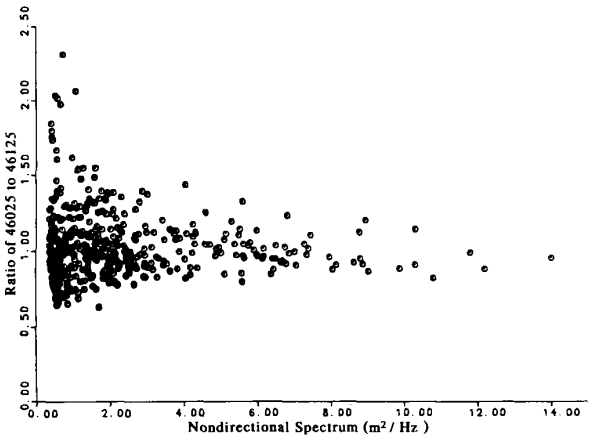

Fig. 2. The ratio of hourly readings during March 1986 of the nondirectional spectrum at 0.07 Hz from a fixed accelerometer (46025) to simultaneous measurements from a vertically stabilized accelerometer (46125) on the same hull. Measurements below three times the estimated electronic noise have been excluded. This illustrates the upward skewing of the distribution at low amplitudes below the spectral peak.

From the analysis in previous sections we can now make a series of predictions on wave-buoy measurements below the spectral peak; we then show that measured data support these predictions. (The instrument signal levels for all data analyzed and presented here were at least 10 dB greater than the noise at the same frequency.)

1) Co-located, strapped-down, and vertically stabilized accelerometers will produce inconsistent results for a wave elevation below the spectral peak when nonlinear wave energy is dominant, with the fixed accelerometer producing the higher, more accurate result. This effect is illustrated in Fig. 2 for data at a particular ocean wave frequency (0.07 Hz).

2) From the properties of co-spectra C_{ij} measured by the vertically stabilized heave sensor and two slope sensors on a pitch/roll wave buoy (labeled 1 and 2, 3, respectively) it follows that

$$u \equiv (C_{22}+C_{33})/(k^2C_{11}) = 1. \tag{12}$$

If S_s and S_h denote slope and height spectral energy measured by the buoy, respectively, then the ratio u should have the approximate dependence

$$u \sim S_s/S_h. \tag{13}$$

Now, if S_h erroneously tends rapidly to zero below the spectral peak because it misses important second-order energy contributions, while S_s still includes second-order energy, then u will exceed unity. This behavior is illustrated in Fig. 4, in which several hourly data records for u are plotted versus frequency. Fig. 3 shows the corresponding nondirectional spectra.

3) As shown in [1], the output of the pitch/roll wave buoy can be expressed as the first five coefficients of a Fourier series for the directional spectrum at each wave frequency:

$$S(f) = a_0/2 + (a_1 \cos\phi + b_1 \sin\phi) + (a_2 \cos 2\phi + b_2 \sin 2\phi) + \cdots \tag{14}$$

where the Fourier coefficients are given in terms of the co- and quad-spectra through the relations

$$a_0 = C_{11}/\pi, \qquad a_1 = Q_{12}/(k\pi), \qquad b_1 = Q_{13}/(k\pi)$$
$$a_2 = (C_{22}-C_{33})/(\pi k^2), \qquad b_2 = 2C_{23}/(\pi k^2). \tag{15}$$

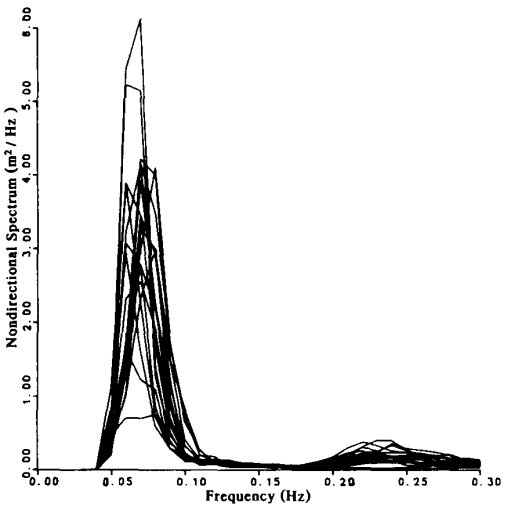

Fig. 3. The nondirectional spectrum obtained hourly from a vertically stabilized accelerometer between 0300Z and 2000Z, May 6, 1986, off Port Hueneme, California. The spectrum corresponds to long-period swell from the Pacific.

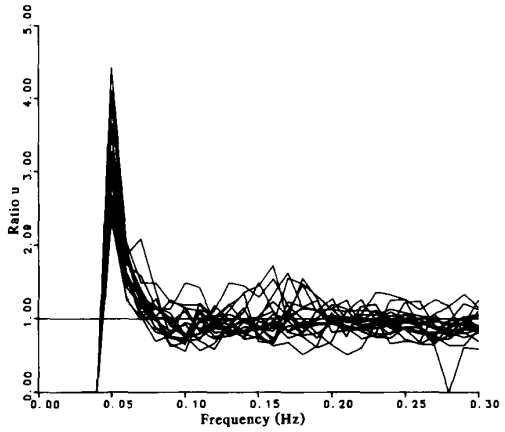

Fig. 4. The ratio u of the height spectrum from the slope sensors to that from the vertically stabilized accelerometer plotted versus frequency. Times and location are the same as for Fig. 3. The value of u has been set to zero at frequencies where the spectral energy is less than 10 dB above the noise level.

As the directional spectrum is necessarily positive, it follows from the Schwarz inequality that the ratios r_1 and r_2, as defined in [3] (for idealized spectra) and repeated here,

$$r_1 = \sqrt{(a_1^2+b_1^2)}/a_0, \qquad r_2 = \sqrt{(a_2^2+b_2^2)}/a_0 \tag{16}$$

are less than unity. However, it follows from the above definitions that r_1 and r_2 depend on the slope and height spectral energy approximately as

$$r_1 \sim \sqrt{(S_s/S_h)}, \qquad r_2 \sim S_s/S_h. \tag{17}$$

Hence in the region below the spectral peak, where nonlinear energy dominates and $S_h \ll S_s$, the instruments mounted on the buoy will indicate that both r_1 and r_2 exceed unity and even further, than r_2 will increase more rapidly than r_1. Fig. 5 shows how these conclusions are verified by the buoy data.

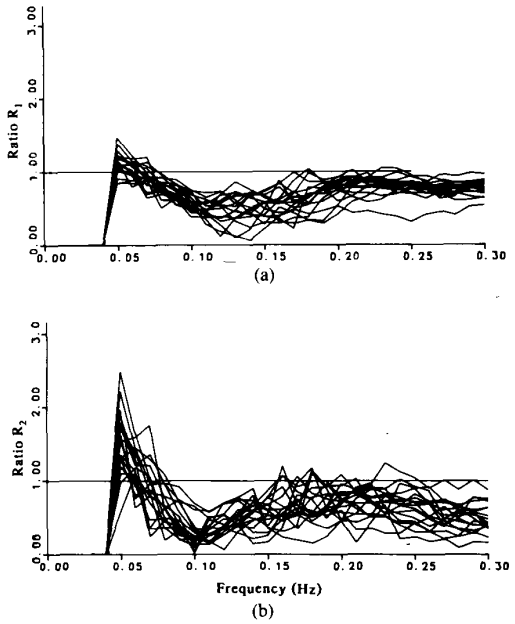

Fig. 5. The ratio r_1 versus frequency (a) and r_2 versus frequency (b). Heave is also here obtained from the vertically stabilized accelerometer. Times and locations are the same as for Fig. 3. The values of r_1 and r_2 have been set to zero when the spectral energy is below the noise level. Note that r_2 increases below the spectral peak more rapidly than r_1, as is expected from equation (17).

V. Conclusions

The pitch/roll buoy has and will continue to provide useful wave-height directional spectral information. Users should be aware, however, that nonlinearities can be expected to produce presently unpredictable biases in height and slope energy of 5–15 percent near and above the spectral peak, and much greater bias below it. Two types are considered here: i) Wave nonlinearities themselves, which will cause bias even in a perfect buoy; and ii) nonlinear constraints within the buoy and mooring hydrodynamic response. Biases produced by both types of nonlinearities studied here increase in severity with the parameter δ, which is the wave slope of the dominant waves.

For many oceanographic applications one can live with a 15 percent measurement bias, while in others (e.g., use as comparison standard for other instruments, design of structures) such biases must be taken into account. This brief analysis also explains the disconcerting failure of directional wave-buoy data presented as r_1 and r_2 to satisfy the Schwarz inequality, as they must; the instrument is *not* malfunctioning; rather, this is the performance one will obtain even from a perfect, free-floating height/slope follower!

Once the equations describing a nonlinear phenomenon are formulated exactly and all parameters affecting the nonlinear response are known (e.g., currents, winds, waves), it is theoretically possible to remove the bias. The above considerations and analysis suggest that these biases may be more easily removed or corrected either: i) In the time domain (i.e., by operation on the time series) before Fourier transforming to the frequency domain; or ii) in the frequency domain by calculating and applying a different calibration factor at each observation time. The efficacy of such methods is presently unknown. Nonetheless, some quantitative improvement in bias reduction can certainly be expected based on more detailed analysis of the nonlinear effects suggested herein.

Acknowledgment

The assistance of NDBC personnel is greatly appreciated.

References

[1] M. S. Longuet-Higgins, D. E. Cartwright, and N. D. Smith, "Observations of the directional spectrum of sea waves using the motions of a floating buoy," in *Ocean Wave Spectra*. Englewood Cliffs, NJ: Prentice-Hall, 1963.

[2] R. H. Stewart, "A discus-hulled wave measuring buoy," in *Ocean Engineering*, vol. 4. New York: Pergamon, 1977, pp. 101–107.

[3] K. E. Steele, J. S.-K. Lau, and Y.-H.L. Hsu, "Theory and application of calibration techniques for an NDBC directional wave measurements buoy," *IEEE J. Oceanic Eng.*, vol. OE-10, no. 4, pp. 382–396, 1985.

[4] *Measuring Ocean Waves*, Proc. Symp. and Workshop on Wave Measurement Tech. Washington, DC: Nat. Acad. Press, 1981.

[5] B. Kinsman, *Wind Waves*, Englewood Cliffs, NJ: Prentice-Hall, 1965.

[6] O. M. Phillips, "On the dynamics of unsteady gravity waves of finite amplitude. Part 1. The elementary interactions," *J. Fluid Mech.*, vol. 9, pp. 193–217, 1960.
——, "...Part 2. Local properties of a random wave field," *J. Fluid Mech.*, vol. 11, pp. 143–155, 1961.

[7] D. E. Barrick and B. L. Weber, "On the nonlinear theory for gravity waves on the ocean's surface. Part I. Derivations," *J. Phys. Oceanogr.*, vol. 7, pp. 3–10, 1977.
——, "...Part 2. Interpretation and applications," *J. Phys. Oceanogr.*, vol. 7, pp. 11–21, 1977.

[8] G. J. Komen, "Nonlinear contributions to the frequency spectrum of wind-generated water waves," *J. Phys. Oceanogr.*, vol. 10, pp. 779–790, 1980.

[9] M. S. Longuet-Higgins, "Accelerations in steep gravity waves," *J. Phys. Oceanogr.*, vol. 15, pp. 1570–1579, 1985.

[10] Y. A. Papadimitrakis, "On the structure of artificially generated water wave trains," *J. Geophys. Res.*, vol. 91, no. C12, pp. 14237–14249, 1986.

[11] K. Hasselmann *et al.*, "Measurements of wind-wave growth and swell decay during the Joint North Sea Project (JONSWAP)," *Erganzungsh. Deut. Hydrograph. Z. Reihe*, vol. A8, no. 12, 1973.

[12] D. E. Barrick, "The role of the gravity-wave dispersion relation in HF radar measurements of the sea surface," *IEEE J. Oceanic Eng.*, vol. OE-11, no. 2, pp. 286–292, 1986.